Direct limits for scalar field dark matter from a gravitational-wave detector

Hartmut Grote (groteh@cardiff.ac.uk)
Cardiff University https://orcid.org/0000-0002-0797-3943
Sander Vermeulen
Cardiff University
Philip Relton
Cardiff University
Vivien Raymond
Cardiff University
Christoph Affeldt
AEI Hannover
Fabio Bergamin
AEI Hannover
Aparna Bisht
AEI Hannover
Marc Brinkmann
AEI Hannover
Karsten Danzmann
Leibniz Universitaet Hannover
Suresh Doravari
AEI Hannover
Volker Kringel
AEI Hannover
James Lough
AEI Hannover https://orcid.org/0000-0002-5160-0239
Harald Lueck
AEI Hannover
Moritz Mehmet
AEI Hannover
Nikhil Mukund
AEI Hannover https://orcid.org/0000-0002-8666-9156
Severin Nadji
AEI Hannover
Emil Schreiber

AEI Hannover
Borja Sorazu
Glasgow University
Kenneth Strain
Glasgow University
Henning Vahlbruch
AEI Hannover
Michael Weinert
AEI Hannover
Benno Willke
AEI Hannover and Leibniz Universitaet Hannover

Physical Sciences - Article

Keywords: dark matter, gravitational-wave detector

Posted Date: March 24th, 2021

DOI: https://doi.org/10.21203/rs.3.rs-322391/v1

Version of Record: A version of this preprint was published at Nature on December 15th, 2021. See the published version at https://doi.org/10.1038/s41586-021-04031-y.

Direct limits for scalar field dark matter from a gravitational-wave detector

Sander M. Vermeulen[1], Philip Relton[1], Hartmut Grote[1],* Vivien Raymond[1], Christoph Affeldt[2], Fabio Bergamin[2], Aparna Bisht[2], Marc Brinkmann[2], Karsten Danzmann[2], Suresh Doravari[2], Volker Kringel[2], James Lough[2], Harald Lück[2], Moritz Mehmet[2], Nikhil Mukund[2], Séverin Nadji[2], Emil Schreiber[2], Borja Sorazu[3], Kenneth A. Strain[2,3], Henning Vahlbruch[2], Michael Weinert[2], and Benno Willke[2]

[1] *Gravity Exploration Institute, Cardiff University, Cardiff CF24 3AA, United Kingdom*

[2] *Max-Planck-Institute for Gravitational Physics and Leibniz University Hannover, Callinstr. 38, 30167 Hannover, Germany and*

[3] *School of Physics and Astronomy, University of Glasgow, Glasgow G12 8QQ, United Kingdom*

(Dated: March 19, 2021)

The nature of dark matter remains unknown to date and several candidate particles are being considered in a dynamically changing research landscape [1]. Scalar field dark matter is a prominent option that is being explored with precision instruments such as atomic clocks and optical cavities [2–8]. Here we report on the first direct search for scalar field dark matter utilising a gravitational-wave detector operating beyond the quantum shot-noise limit. We set new upper limits for the coupling constants of scalar field dark matter as a function of its mass by excluding the presence of signals that would be produced through the direct coupling of this dark matter to the beamsplitter of the GEO 600 interferometer. The new constraints improve upon bounds from previous direct searches by more than six orders of magnitude and are more stringent than limits obtained in tests of the equivalence principle by one order of magnitude. Our work demonstrates that scalar field dark matter can be probed or constrained with direct searches using gravitational-wave detectors and highlights the potential of quantum-enhanced interferometry for dark matter detection.

I. INTRODUCTION

Laser interferometers have exquisite sensitivity to minute length changes of space and have facilitated many gravitational-wave detections over the last years [9, 10]. In addition to their revolutionary merit in astrophysics, the detection of gravitational waves has also shed light on fundamental physics questions and several links may exist between gravitational waves and dark matter [11]. Due to their excellent sensitivity at or beyond quantum limits, gravitational-wave detectors (or precision interferometers of a similar type) can be used directly for fundamental physics, without the mediation of gravitational waves. Examples include a possible search for vacuum birefringence [12] and the search for signatures of quantum gravity [13–15]. Several ideas have been put forward as to how different candidates of dark matter can directly couple to gravitational-wave detectors, ranging from scalar field dark matter [4, 16] to dark photon dark matter [17], and to clumpy dark matter coupling gravitationally or through an additional Yukawa force [18]. Upper limits for dark photon dark matter have already been set in a small mass band using data from the first observational run (O1) of the Advanced LIGO gravitational-wave detectors [19].

In this work we conduct the first direct search for scalar field dark matter using a gravitational-wave detector, the quantum-enhanced GEO 600 interferometer, and set new upper limits on the parameters of such dark matter.

* Correspondence email address: groteh@cardiff.ac.uk

II. THEORY

Models of weakly coupled low-mass ($\ll 1\,\mathrm{eV}$) scalar dark matter (DM) predict that such particles would manifest as a coherently oscillating field [2, 4],

$$\phi(t,\vec{r}) = \phi_0 \cos\left(\omega_\phi t - \vec{k}_\phi \cdot \vec{r}\right), \tag{1}$$

where $\omega_\phi = (m_\phi c^2)/\hbar$ is the angular Compton frequency, and $\vec{k}_\phi = (m_\phi \vec{v}_{\mathrm{obs}})/\hbar$ is the wave vector, with m_ϕ the mass of the field and $\vec{v}_{\mathrm{obs}}$ the velocity relative to the observer. The amplitude of the field can be set as $\phi_0 = (\hbar\sqrt{2\rho_{\mathrm{CDM}}})/(m_\phi c)$ under the assumption that this DM field constitutes the local dark matter density ρ_{CDM} [20].

Moreover, the DM would be virialised in the galactic gravity potential, leading to a Maxwell-Boltzmann-like distribution of velocities $\vec{v}_{\mathrm{obs}}$. As non-zero velocities produce a Doppler-shift of the observed DM field frequency, this virialisation results in the DM field having a finite coherence time or, equivalently, a spread in observed frequency (linewidth) $\Delta\omega_{\mathrm{obs}}/\omega_{\mathrm{obs}} \sim 10^{-6}$ [17, 21]. The observed DM frequency is further modulated by the motion of the Earth with respect to the galactic DM halo.

This scalar DM field ϕ could couple to the fields of the Standard Model (SM) in numerous ways. Such a

coupling, sometimes called a 'portal', is modelled by the addition of a parameterised interaction term to the SM Lagrangian [22, 23]. In this paper, we consider linear interaction terms involving the electron rest mass m_e and the electromagnetic field tensor $F_{\mu\nu}$:

$$\mathcal{L}_{int} = \frac{\phi}{\Lambda_\gamma}\frac{F_{\mu\nu}F^{\mu\nu}}{4} - \frac{\phi}{\Lambda_e} m_e \bar{\psi}_e \psi_e, \qquad (2)$$

where ψ_e, $\bar{\psi}_e$ are the SM electron field and its Dirac conjugate, and Λ_γ, Λ_e parameterise the coupling. The addition of these terms to the SM Lagrangian entails relative changes of the fine structure constant and the electron rest mass [4]. It can be shown that such a change of these fundamental constants causes corresponding changes in the size l and refractive index n of a solid [16].

Laser interferometers for gravitational-wave (GW) detection are modified Michelson interferometers with exquisite sensitivity to differential changes in the optical path length of their arms. The thin cylindrical beamsplitter in such an instrument interacts asymmetrically with light from the two arms, as the front surface has a 50% reflectivity and the back surface has an anti-reflective coating. Therefore, a change in the size (δl) and index of refraction (δn) of the beamsplitter affects the two arms differently, and produces an effective difference in the optical path lengths of the arms $L_{x,y}$

$$\delta(L_x - L_y) \approx \sqrt{2}\left[\left(n - \frac{1}{2}\right)\delta l + l\delta n\right].^{1} \qquad (3)$$

The mirrors in the arms of GW interferometers would also undergo changes in their size and index of refraction, but as the wavelength of the DM field is much greater than the distance between the arm mirrors ($\lambda_\phi/L \gtrsim 10^3$) for all frequencies of interest, and because the mirrors have roughly the same thickness, the effect is almost equal in both arms and thus does not produce a dominant signal.

The interferometer most sensitive to potential DM signals is the GEO 600 detector, as it has the highest sensitivity to optical phase differences between the two arms. The squeezed vacuum states of light currently employed in this instrument allow for a world-record quantum noise reduction of 6 dB [24]. Although other GW detectors (LIGO/Virgo) are more sensitive to gravitational waves through the use of Fabry-Pérot cavities in the arms, these do not boost their sensitivity to signals induced at the beamsplitter, so their relative sensitivity to scalar DM is lower [16].

[1] This expression includes a correction to Eq. 17 in [16]. In addition, a geometrical correction factor (< 10%) from Snell's law is applied to Eqs. 3 and 4 for calculating the results below.

From Eqs. 1-3 it follows that an oscillating scalar dark matter field is expected to produce a Doppler-shifted and -broadened signal in an interferometer of the form

$$\delta(L_x - L_y) \approx \left(\frac{1}{\Lambda_\gamma} + \frac{1}{\Lambda_e}\right)\left(\frac{n\,l\,\hbar\sqrt{2\,\rho_{\rm CDM}}}{m_\phi\,c}\right)\cos\left(\omega_{\rm obs}t\right), \qquad (4)$$

and examining data from the GEO 600 detector for the presence of such a signal therefore allows us to set constraints on the properties of scalar dark matter.

III. RESULTS

The GEO 600 interferometer [25] has been in joint observing runs with the Advanced LIGO detectors since 2015, primarily to look for gravitational waves. We performed spectral analysis on seven $T \sim 10^5$ s segments of strain data from the GEO 600 interferometer (acquired in 2016 and 2019) using a modified version of the LPSD technique [26], which was designed to produce spectra with logarithmically spaced frequencies. Using this algorithm to perform discrete Fourier transforms (DFT) with a frequency dependent length, we created spectra in which each frequency bin was made to have a width equal to the Doppler-broadened linewidth of potential DM signals. This method yields in theory the maximum attainable signal-to-noise ratio (SNR) given a certain amount of data (see Sec. V) [21, 27]. A matched filtering approach is not feasible as the phase of the signal varies stochastically.

We analysed the amplitude spectra of all seven strain data segments for the presence of DM signals by looking for significant peaks in the underlying noise. Peaks were considered candidates when there was a less than 1% probability of the local maximum being due to noise, where we compensated for the look-elsewhere effect using a large trial factor ($\sim 10^6$).

This analysis found $\sim 10^4$ peaks above the 95% confidence level ($\gtrsim 5.6\sigma$), where the total error includes a frequency dependent amplitude calibration error of up to 30% inherent to GEO 600 data [28]. The frequency and amplitude stability of the peaks in time was then evaluated by cross-checking all candidates between spectra. Candidate peaks were rejected if their centre frequencies differed between spectra by more than the Doppler shift expected from the Earth's motion around the Sun [29]. Peaks were also rejected if their amplitude changed significantly ($\gtrsim 5\sigma$) between spectra.

Using this procedure, we eliminated all but 14 candidate peaks, where the vast majority (> 99%) of peaks were rejected because they did not appear in all data sets within the centre frequency tolerance.

These 14 candidate peaks were subjected to further analysis to investigate if their properties matched that

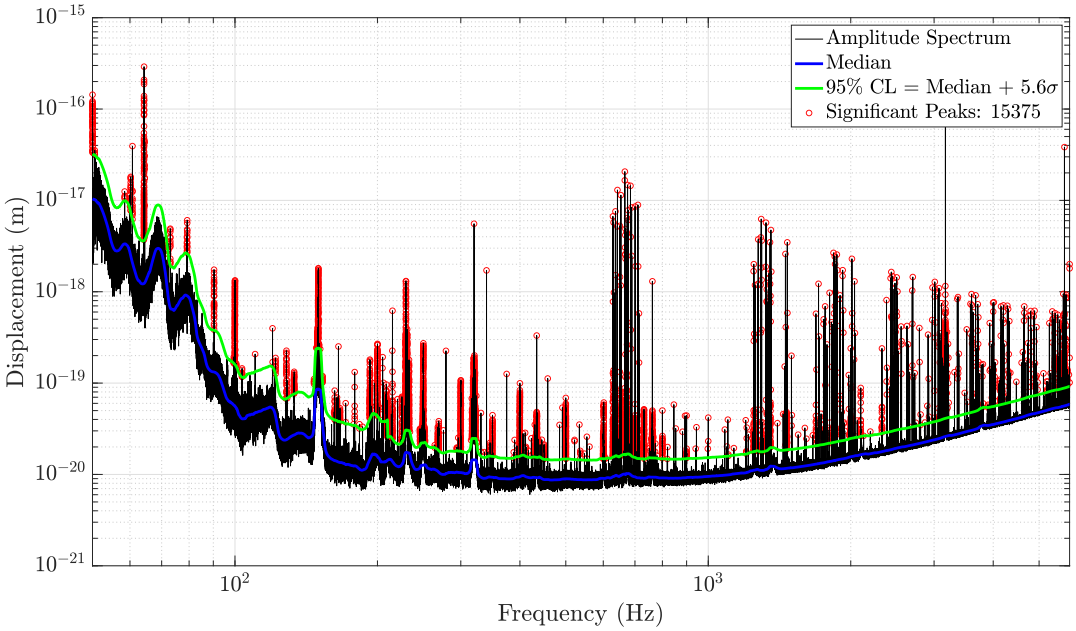

Figure 1. A typical amplitude spectrum (black) produced with frequency bins that are tuned to the expected dark matter linewidth using the modified LPSD technique. The noise spectrum was estimated at each frequency bin from neighbouring bins to yield the local noise median (blue) and 95% confidence level (green). Peaks (red) above this confidence level were considered candidates for DM signals and subjected to follow-up analysis.

of a DM signal. 13 of the peaks were found to have insufficient width to be caused by DM ($\Delta f_{\rm peak}/\Delta f_{\rm DM} \lesssim 10$, see Sec. V). The remaining candidate peak was also ultimately rejected, as although it appeared to have sufficient frequency spread to be a DM signal, additional analysis showed this signal has a coherence time much greater than that expected for a DM signal of that frequency ($\tau_c^{\rm peak}/\tau_c^{\rm DM} > 10$, see Sec. V).

Having determined that all significant peaks in the amplitude spectrum are not caused by scalar field DM, we set constraints on the parameters of such dark matter at a 95% confidence level (corresponding to 5.6σ above the noise floor), using Eq. 4. The results for the photon and electron coupling parameters as a function of field mass are given in Fig. 2.

These results assume a local dark matter density $\rho_{\rm CDM} = 0.3$ GeV/cm^3. This is a conservative estimate; slightly higher values ($\rho_{\rm CDM} \approx 0.4$ GeV/cm^3) are reported in literature for the standard smooth DM halo model [29]. Models in which DM forms a relaxion halo [34, 35] predict local DM overdensities of up to $\rho_{\rm RH}/\rho_{\rm CDM} \leq 10^{16}$ [36]. Our results impose significantly more stringent constraints on the coupling constants for higher assumed values of the DM density $\rho_{\rm A} > \rho_{\rm CDM}$: the constraint becomes more stringent by a factor $(\rho_{\rm A}/\rho_{\rm CDM})^{1/2}$ (see Eq. 4).

IV. CONCLUSIONS

In this paper, we presented the first search for signals of scalar field dark matter in the data of a gravitational-wave detector. Scalar field dark matter would cause oscillations of the size and index of refraction of the beamsplitter in such an interferometer, which produces an oscillatory signal at a frequency set by the mass of the dark matter particle. As exquisite classical noise mitigation is employed in gravitational-wave detectors, quantum technologies such as squeezed light can provide a major increase in sensitivity. Such technologies facilitate measurements beyond the shot-noise quantum limit, and yield unprecedented sensitivity to scalar field dark matter in a wide mass range. In addition, by tuning the frequency bin widths to the expected dark matter linewidth, our spectral analysis method improves on the analyses used in previous work that set constraints on dark photons using data from gravitational-wave detectors [17, 19], and other searches for scalar fields in frequency space. In contrast to these other efforts, the spectral analysis presented here yields the optimal signal-to-noise ratio for potential dark matter signals across the full frequency range.

We excluded the presence of such signals in the data of the GEO 600 gravitational-wave detector, thereby setting new upper limits on dark matter couplings at up to $\Lambda_{e,\gamma} = 3 \cdot 10^{19}$ GeV for dark matter masses between

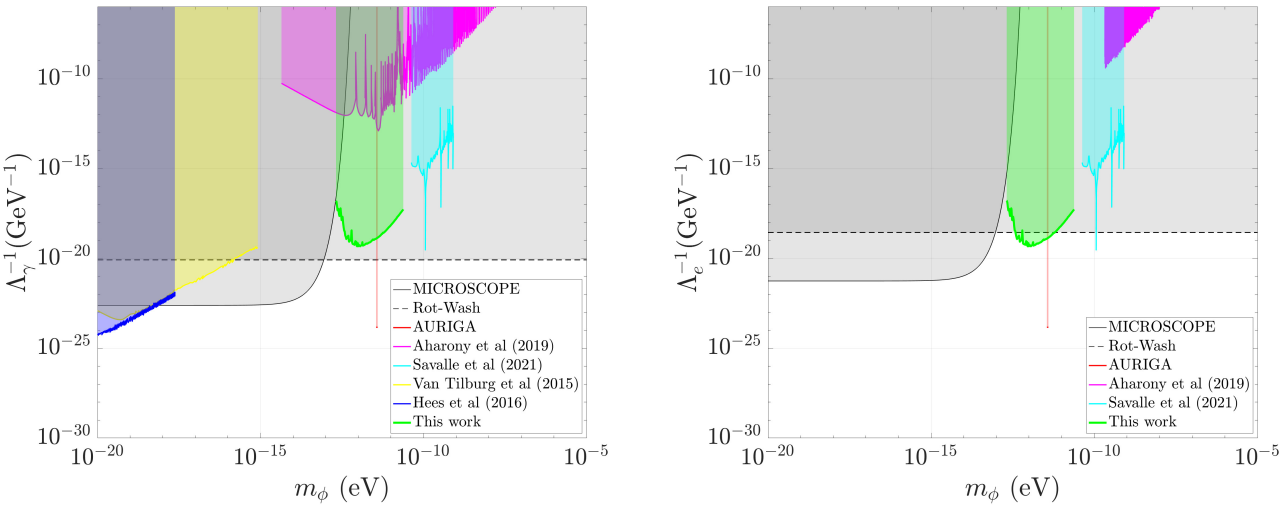

Figure 2. Constraints on the coupling parameters Λ_γ, Λ_e of scalar field DM interacting linearly with respectively the electromagnetic (left) and electron field (right) as a function of the field's mass m_ϕ. The green regions denote the parameter space excluded at a 95% confidence level in the current study through the spectral analysis of data from the GEO 600 GW detector. The thin red regions show existing constraints of scalar field DM obtained with the resonant-mass AURIGA detector [30]. The other coloured regions represent previous constraint from other direct searches [5, 6, 8, 31]. The grey regions correspond to previous constraints on general fifth-forces from tests of the equivalence principle [7] in earth-based (Rot-Wash) [32] and space-based (MICROSCOPE) [33] experiments.

10^{-13} and 10^{-11} eV. The new constraints improve upon the current limits obtained with atomic spectroscopy experiments [31] by more than six orders of magnitude, and are an order of magnitude more stringent than previous bounds from tests of the equivalence principle [23].

Tighter constraints on scalar field dark matter in various mass ranges can be set in the future using new yet-to-be-built gravitational-wave detectors or other similar precision interferometers. Using the same methods as in this work these instruments would allow new limits to be set across their characteristic sensitive frequency range. In addition, by slightly modifying the optics in such interferometers, e.g. by using mirrors of different thicknesses in each interferometer arm, their sensitivity to scalar field dark matter could be improved even further [16]. Through the reduction of losses, quantum technologies such as squeezed light are also expected to improve, allowing for ever-increasing noise mitigation [37]. These and other forthcoming technological advances make precision interferometers operating beyond quantum limits indispensable tools for dark matter detection and fundamental physics in general.

ACKNOWLEDGEMENTS

The authors thank Yevgeny Stadnik and Yuta Michimura for valuable discussion and comments on this work. We thank Duncan Macleod and Paul Hopkins for significant programming assistance, and Michael Tröbs and Gerhard Heinzel for permission to use their LPSD code. The authors are grateful for support from the Science and Technology Facilities Council (STFC), grants ST/T006331/1, ST/I006285/1, and ST/L000946/1, the Leverhulme Trust, grant RPG-2019-022, and the Universities of Cardiff and Glasgow in the United Kingdom, the Bundesministerium für Bildung und Forschung, the state of Lower Saxony in Germany, the Max Planck Society, Leibniz Universität Hannover, and Deutsche Forschungsgemeinschaft (DFG, German Research Foundation) under Germany's Excellence Strategy EXC 2123 QuantumFrontiers 390837967. This work also was partly supported by DFG grant SFB/ Transregio 7 Gravitational Wave Astronomy. We further thank Walter Grass for his years of expert infrastructure support for GEO 600. This document has been assigned LIGO document number LIGO-P2100053.

AUTHOR CONTRIBUTIONS

S.M.V. and P.R. have analysed the data and compiled the results; H.G. has instigated this work and S.M.V. and H.G. have written the manuscript; V.R has given critical input to the analysis. C.A., J.L. and K.D. have lead the GEO 600 instrument group during the period

where data for this work was acquired. F.B., A.B, S.D. H.L., N.M., S.N., E.S, B.S., K.A.S, M.B., V.K, and M.W. have worked on the instrument in different capacities required to achieve sensitivity and extended run duration; B.W. has provided laser expertise and H.V. and M.M. have build the squeezed-light source.

V. METHODS

A. Spectral estimation

Spectral analysis was performed using a modified version of the LPSD technique [26]. This technique is designed to produce spectral estimates with logarithmically spaced frequencies, and thus allows for the production of spectral estimates with a frequency-dependent bin width. Using this technique, we subdivided the $\sim 10^5$ s data segments into

$$N_f = \left\lfloor \frac{T - \tau_{\rm coh}(f)}{\tau_{\rm coh}(f)(1-\xi)} + 1 \right\rfloor \tag{5}$$

smaller overlapping subsegments $S_f^k(t)$ with a length equal to the expected coherence time $\tau_{\rm coh}(f)$, of a dark matter (DM) signal at a frequency f, where $\xi \in [0,1]$ is the fractional overlap of the subsegments, and $k \in [1, N_f]$). As the expected coherence time and linewidth is frequency dependent, this subdivision is unique for every frequency of interest. After subdivision, the subsegments were multiplied with a Kaiser window function $W_f(t)$ and subjected to a DFT at a single frequency:

$$a^k(f) = \sum_{t=0}^{T_{\rm DFT}} W_f(t)\, S_f^k(t)\, \mathrm{e}^{2\pi i f t}, \tag{6}$$

with $T_{\rm DFT} = \tau_{\rm coh}(f)$, where $a^k(f)$ is thus the complex spectral estimate at frequency f for the $k^{\rm th}$ subsegment. Frequency points are chosen by dividing the interval between the chosen minimum frequency (50 Hz) and the Nyquist frequency (≈ 8.2 kHz) by the DM linewidth, and then rounding the resulting number of bins to the nearest integer to set the final frequency points and bin widths. The absolute squared magnitudes $|a^k(f)|^2$ are averaged over the subsegments to obtain the power spectrum

$$P(f) = \frac{C}{N_f} \sum_{k=1}^{N_f} |a^k(f)|^2, \tag{7}$$

where C is a normalisation factor. The amplitude spectrum $A(f) = \sqrt{P(f)}$ created in this way comprises $\approx 5 \cdot 10^6$ frequency bins between 50 Hz and 6 kHz.

The SNR for DM signals in such a spectrum is optimal given a certain amount of data (see Sec. V D), and can only be further improved by analysing more data. Additional data would allow for more averaging, which decreases the variance of the spectrum as the square root of the amount of data, such that the sensitivity approaches the noise floor. The noise floor can be lowered using longer DFT lengths at the cost of reduced SNR, but this is subject to severely diminishing returns; the sensitivity can only be improved by a factor proportional to the fourth root of the amount of data needed [21] (and the computation time scales with the product of DFT length and the amount of data [26]). Computation times for the spectra used in this work are ~ 10 s per frequency bin for each $\sim 10^5$ s data set, or $\sim 10^4$ CPU hours per spectrum.

B. Estimation of noise statistics

The local noise parameters were estimated at every frequency bin from $w = 5 \cdot 10^4$ neighbouring bins. This method allows the underlying noise distribution to be estimated in a way that is independent of narrow ($\ll w$) spectral features (such as those due to mechanical excitation of the mirror suspensions), under the assumption that the underlying noise spectrum is locally flat (that is, the auto-correlation length of the noise spectrum is assumed to be $\gg w$). The choice of w thus represents a trade-off between erroneously assuming instrumental spectral artefacts or signals to be features of the underlying noise spectrum versus erroneously assuming features of the underlying noise spectrum to be instrumental spectral artefacts or signals.

C. Follow-up analysis of candidates

As mentioned above, 14 candidate peaks remained after cross-checking spectra taken at different times. 13 of these peaks were found to have insufficient width to be DM signals. Further investigation of each of these candidates found that shifting the bin centre frequencies by an amount much smaller than the expected linewidth of DM signals of that frequency and amplitude and recomputing the spectra did not reproduce the peak. Additional work revealed these 13 candidate peaks were not present in spectra created using the same data and the same LPSD algorithm implemented in a different programming language, whereas the noise floor and other spectral features were reproduced identically. These peaks are therefore likely artefacts of the numerical implementation of the LPSD technique.

The coherence time of the single remaining candidate peak was probed by evaluating its height in the amplitude spectrum as a function of the DFT length (see Sec. V D). The height of the peak did not decrease for DFT lengths more than an order of magnitude greater than the expected DM coherence time, evidencing a coherence time much greater than that expected for a DM signal of that frequency, and the peak was therefore rejected.

D. Validation of methods

To validate several aspects of our analysis methods, we simulated DM signals and injected them into sets of real and simulated data. The DM signals were created by superposing $\sim 10^2$ sinusoids at frequencies linearly spaced around a centre frequency (the simulated Doppler-shifted DM Compton frequency), where the amplitude of each sinusoid is given

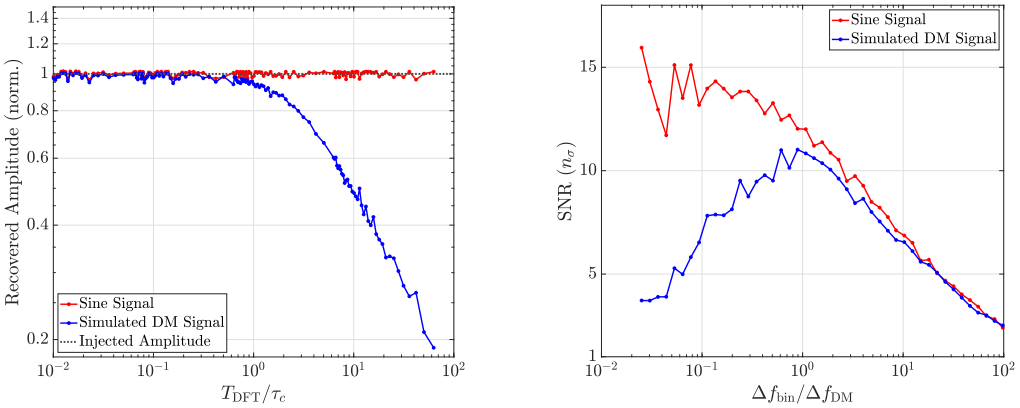

Figure 3. The spectral amplitude (left) and signal-to-noise ratio (SNR, right) of a simulated DM signal (blue) and monochromatic sine wave (red) as recovered from spectra created using different frequency bin widths ($\Delta f_{\mathrm{bin}} = 1/T_{\mathrm{DFT}}$). The plotted recovered amplitude is normalised by the injected amplitude. The SNR (n_σ) is measured as the difference between the signal amplitude and the noise amplitude divided by the standard deviation of the noise. The appearance of a maximum for the SNR as shown on the right is a direct consequence of both the decrease of the recovered amplitude of signals with limited coherence (as shown on the left) and the scaling of white Gaussian noise with increasing integration time. The plot on the left was produced by injecting a simulated dark matter signal and a perfect sine into a segment of GEO 600 data and creating spectra using the modified LPSD technique described above. The plot on the right was made by injecting the same signals into white Gaussian noise and creating spectra using Welch's method. Note that for any single bin and for equal T_{DFT} the spectral estimate obtained with the LPSD method (Eq. 6) is mathematically equal to that obtained with Welch's method.

by the quasi-Maxwellian DM line shape proposed in [21] scaled by a simulated DM coupling constant; the relative phases of the sinusoids are randomised to capture the thermalisation of the scalar field DM.

To test the spectral estimation, signal search, and candidate rejection, a blind injection of simulated DM signals into several GEO 600 data sets was performed, where the frequency, amplitude, and number of signals was masked to the authors. All injected signals were recovered at their Compton frequency and at an amplitude corresponding to the hypothetical coupling constant, and were subsequently identified through cross-checks between spectra as persistent candidate DM signals.

The formerly proposed [17, 21] and herein utilised condition of setting the frequency bin widths equal to the expected DM line width for attaining optimal SNR was tested using simulated DM signals as well. Mock DM signals and monochromatic sine signals were injected into real GEO 600 data and Gaussian noise, and spectra were made for which the width of the frequency bins Δf_{bin} (and correspondingly the length of the DFTs T_{DFT}) was varied over four orders of magnitude. The recovered amplitude of signals injected into GEO 600 data in spectra created using the LPSD algorithm is plotted in Fig. 3 (left). This shows that the recovered amplitude of signals starts to decrease as the DFT length exceeds the coherence time (a monochromatic sine has infinite coherence time), and validates the rejection of the remaining candidate signal above as its amplitude was found to be roughly constant for $T_{\mathrm{DFT}}/\tau_c > 10$. The recovered SNR of signals injected into Gaussian noise in spectra created using Welch's method [38] is plotted in Fig. 3 (right), which confirms that the SNR is maximal when the frequency bin width is roughly equal to the full-width at half-maximum Δf_{DM} of the spectral line shape of the signal. This is a consequence of the aforementioned decrease in recovered amplitude for smaller bin widths and the scaling of white Gaussian noise.

VI. DATA AVAILABILITY

The upper limit data in Fig. 2 and intermediate results, such as the spectrum in Fig. 1, are available from the corresponding author upon reasonable request. The raw data used for the full analysis comprises about 80 GB and is available from the corresponding author upon reasonable request.

VII. CODE AVAILABILITY

The custom codes used to produce the results presented in this manuscript are available from the corresponding author upon reasonable request.

[1] G. Bertone and T. Tait, "A new era in the search for dark matter," *Nature*, vol. 562, pp. 51–56, 2018.

[2] A. Arvanitaki, J. Huang, and K. Van Tilburg, "Searching for dilaton dark matter with atomic clocks," *Physi-*

cal Review D, vol. 91, no. 1, p. 015015, 2015.

[3] A. Derevianko and M. Pospelov, "Hunting for topological dark matter with atomic clocks," *Nature Physics*, vol. 10, no. 12, pp. 933–936, 2014.

[4] Y. V. Stadnik and V. V. Flambaum, "Can dark matter induce cosmological evolution of the fundamental constants of nature?," *Physical Review Letters*, vol. 115, no. 20, p. 201301, 2015.

[5] K. Van Tilburg, N. Leefer, L. Bougas, and D. Budker, "Search for Ultralight Scalar Dark Matter with Atomic Spectroscopy," *Physical Review Letters*, vol. 115, no. 1, p. 011802, 2015.

[6] A. Hees, J. Guéna, M. Abgrall, S. Bize, and P. Wolf, "Searching for an oscillating massive scalar field as a dark matter candidate using atomic hyperfine frequency comparisons," *Physical Review Letters*, vol. 117, no. 6, p. 061301, 2016.

[7] N. Leefer, A. Gerhardus, D. Budker, V. Flambaum, and Y. Stadnik, "Search for the Effect of Massive Bodies on Atomic Spectra and Constraints on Yukawa-Type Interactions of Scalar Particles," *Physical Review Letters*, vol. 117, no. 27, p. 271601, 2016.

[8] E. Savalle *et al.*, "Searching for dark matter with an unequal delay interferometer," *arXiv:2006.07055*, 2021.

[9] B. P. Abbott *et al.*, "Gwtc-1: A gravitational-wave transient catalog of compact binary mergers observed by LIGO and Virgo during the first and second observing runs," *Phys. Rev. X*, vol. 9, p. 031040, 2019.

[10] B. P. Abbott *et al.*, "Gwtc-2: Compact binary coalescences observed by LIGO and Virgo during the first half of the third observing run," *arxiv 2010.14527*, 2020.

[11] G. Bertone *et al.*, "Gravitational wave probes of dark matter: challenges and opportunities," *SciPost Phys. Core*, vol. 3, p. 7, 2020.

[12] H. Grote, "On the possibility of vacuum QED measurements with gravitational wave detectors," *Phys. Rev. D*, vol. 91, p. 022002, 2015.

[13] A. S. Chou *et al.*, "First measurements of high frequency cross-spectra from a pair of large michelson interferometers," *Phys. Rev. Lett.*, vol. 117, p. 111102, 2016.

[14] E. P. Verlinde and K. M. Zurek, "Observational signatures of quantum gravity in interferometers," *arxiv 1902.08207*, 2019.

[15] S. M. Vermeulen *et al.*, "An experiment for observing quantum gravity phenomena using twin table-top 3D interferometers," *Classical and Quantum Gravity*, 2021.

[16] H. Grote and Y. V. Stadnik, "Novel signatures of dark-matter in laser-interferometric gravitational-wave detectors," *Phys. Rev. Research*, vol. 1, p. 033187, 2019.

[17] A. Pierce, K. Riles, and Y. Zhao, "Searching for dark photon dark matter with gravitational wave detectors," *Physical Review Letters*, vol. 121, no. 6, p. 061102, 2018.

[18] E. D. Hall, R. X. Adhikari, V. V. Frolov, H. Müller, and M. Pospelov, "Laser interferometers as dark matter detectors," *Phys. Rev. D*, vol. 98, p. 083019, 2018.

[19] H.-K. Guo, K. Riles, F.-W. Yang, and Y. Zhao, "Searching for dark photon dark matter in LIGO O1 data," *Communications Physics*, vol. 2, 2019.

[20] J. I. Read, "The Local Dark Matter Density," *arXiv:1404.1938*, 2014.

[21] A. Derevianko, "Detecting dark matter waves with precision measurement tools," *Physical Review A*, vol. 97, no. 4, p. 042506, 2018.

[22] A. Ringwald, "Exploring the role of axions and other WISPs in the dark universe," *arXiv:1210.5081*, 2012.

[23] A. Hees, O. Minazzoli, E. Savalle, Y. V. Stadnik, and P. Wolf, "Violation of the equivalence principle from light scalar dark matter," *Physical Review D*, vol. 98, no. 6, p. 064051, 2018.

[24] J. Lough *et al.*, "First demonstration of 6 db quantum noise reduction in a kilometer scale gravitational wave observatory," *Phys. Rev. Lett.*, vol. 126, p. 041102, 2021.

[25] K. L. Dooley *et al.*, "GEO 600 and the GEO-HF upgrade program: successes and challenges," *Classical and Quantum Gravity*, vol. 33, no. 7, p. 075009, 2016.

[26] M. Tröbs and G. Heinzel, "Improved spectrum estimation from digitized time series on a logarithmic frequency axis," *Measurement*, vol. 39, no. 2, pp. 120–129, 2006.

[27] A. L. Miller *et al.*, "Adapting a semi-coherent method to directly detect dark photon dark matter interacting with gravitational-wave interferometers," *arXiv:2010.01925*, 2020.

[28] B. P. Abbott *et al.*, "Properties of the binary neutron star merger gw170817," *Phys. Rev. X*, vol. 9, p. 011001, 2019.

[29] K. Freese, M. Lisanti, and C. Savage, "Annual modulation of dark matter: A review," *Reviews of Modern Physics*, vol. 85, no. 4, pp. 1561–1581, 2013.

[30] A. Branca *et al.*, "Search for an Ultralight Scalar Dark Matter Candidate with the AURIGA Detector," *Physical Review Letters*, vol. 118, no. 2, p. 021302, 2017.

[31] S. Aharony *et al.*, "Constraining Rapidly Oscillating Scalar Dark Matter Using Dynamic Decoupling," *arXiv:1902.02788*, 2019.

[32] G. L. Smith *et al.*, "Short-range tests of the equivalence principle," *Physical Review D*, vol. 61, no. 2, p. 022001, 1999.

[33] J. Bergé *et al.*, "MICROSCOPE Mission: First Constraints on the Violation of the Weak Equivalence Principle by a Light Scalar Dilaton," *Physical Review Letters*, vol. 120, no. 14, p. 141101, 2018.

[34] P. W. Graham, D. E. Kaplan, and S. Rajendran, "Cosmological Relaxation of the Electroweak Scale," *Physical Review Letters*, vol. 115, no. 22, p. 221801, 2015.

[35] E. W. Kolb and I. I. Tkachev, "Axion miniclusters and Bose stars," *Physical Review Letters*, vol. 71, no. 19, pp. 3051–3054, 1993.

[36] E. Savalle *et al.*, "Novel approaches to dark-matter detection using space-time separated clocks," *arXiv:1902.07192*, 2019.

[37] S. T. Pradyumna *et al.*, "Twin beam quantum-enhanced correlated interferometry for testing fundamental physics," *Communications Physics*, vol. 3, no. 1, p. 104, 2020.

[38] P. Welch, "The use of fast fourier transform for the estimation of power spectra: A method based on time averaging over short, modified periodograms," *IEEE Transactions on Audio and Electroacoustics*, vol. 15, no. 2, pp. 70–73, 1967.

Figures

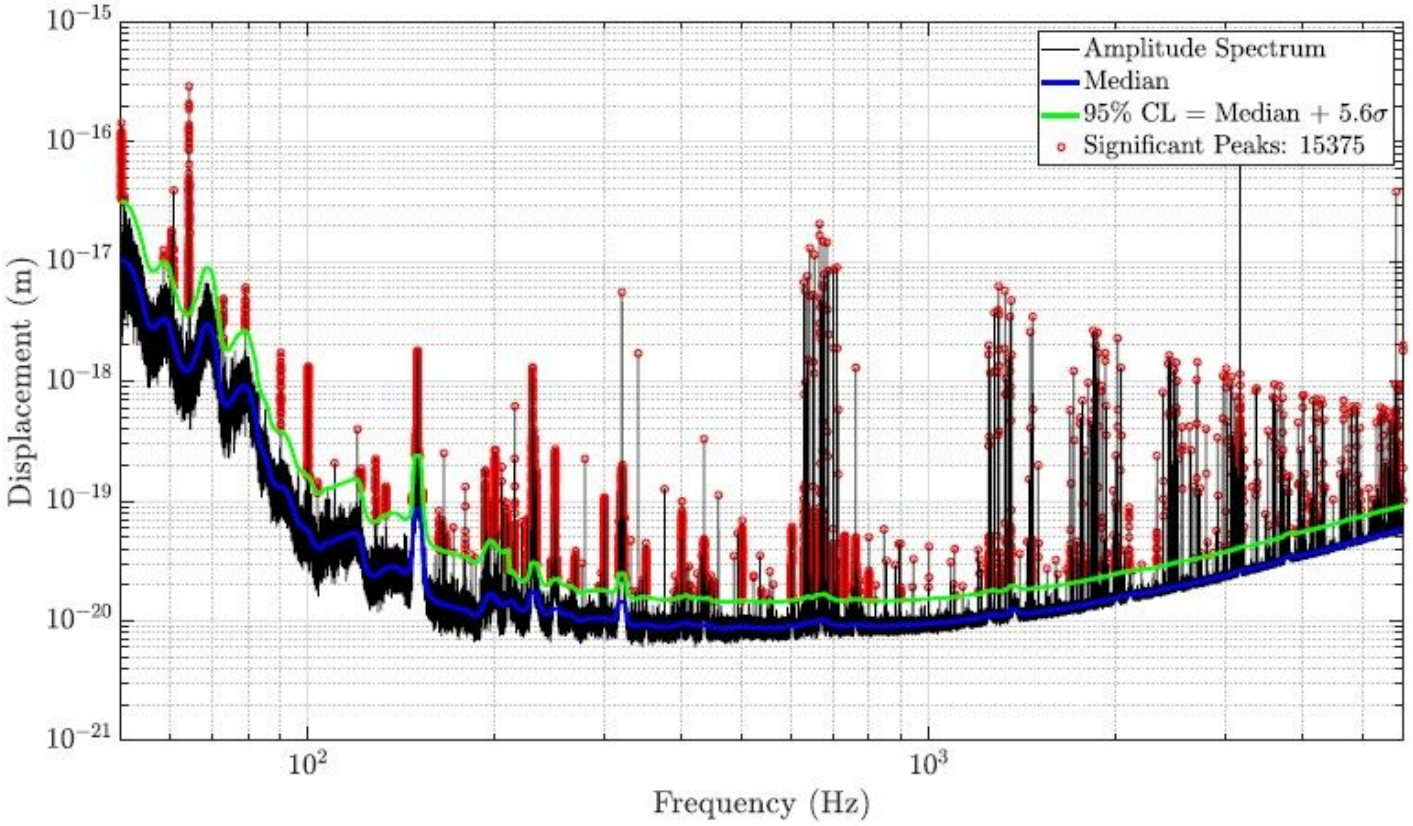

Figure 1

A typical amplitude spectrum (black) produced with frequency bins that are tuned to the expected dark matter linewidth using the modified LPSD technique. The noise spectrum was estimated at each frequency bin from neighbouring bins to yield the local noise median (blue) and 95% confidence level (green). Peaks (red) above this confidence level were considered candidates for DM signals and subjected to follow-up analysis.

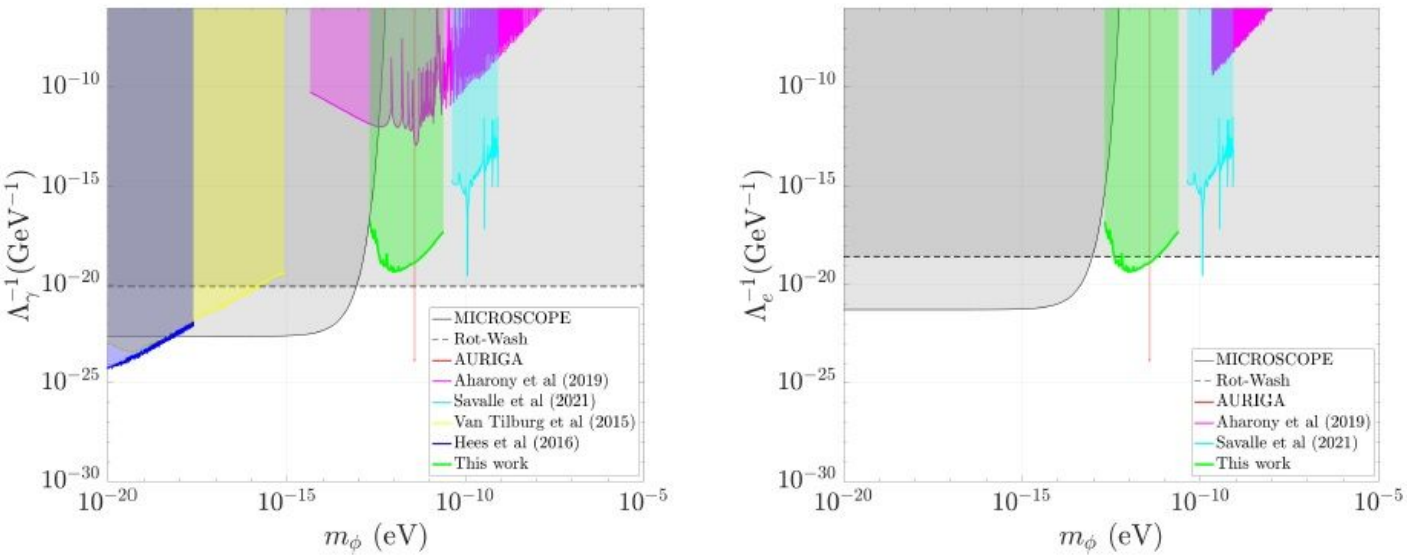

Figure 2

Constraints on the coupling parameters A , Ae of scalar field DM interacting linearly with respectively the electromagnetic (left) and electron field (right) as a function of the field's mass mo. The green regions denote the parameter space excluded at a 95% confidence level in the current study through the spectral analysis of data from the GEO600 GW detector. The thin red regions show existing constraints of scalar field DM obtained with the resonant-mass AURIGA detector [30]. The other coloured regions represent previous constraint from other direct searches [5, 6, 8, 31]. The grey regions correspond to previous constraints on general fifth-forces from tests of the equivalence principle [7] in earth-based (Rot-Wash) [32] and space-based (MICROSCOPE) [33] experiments.

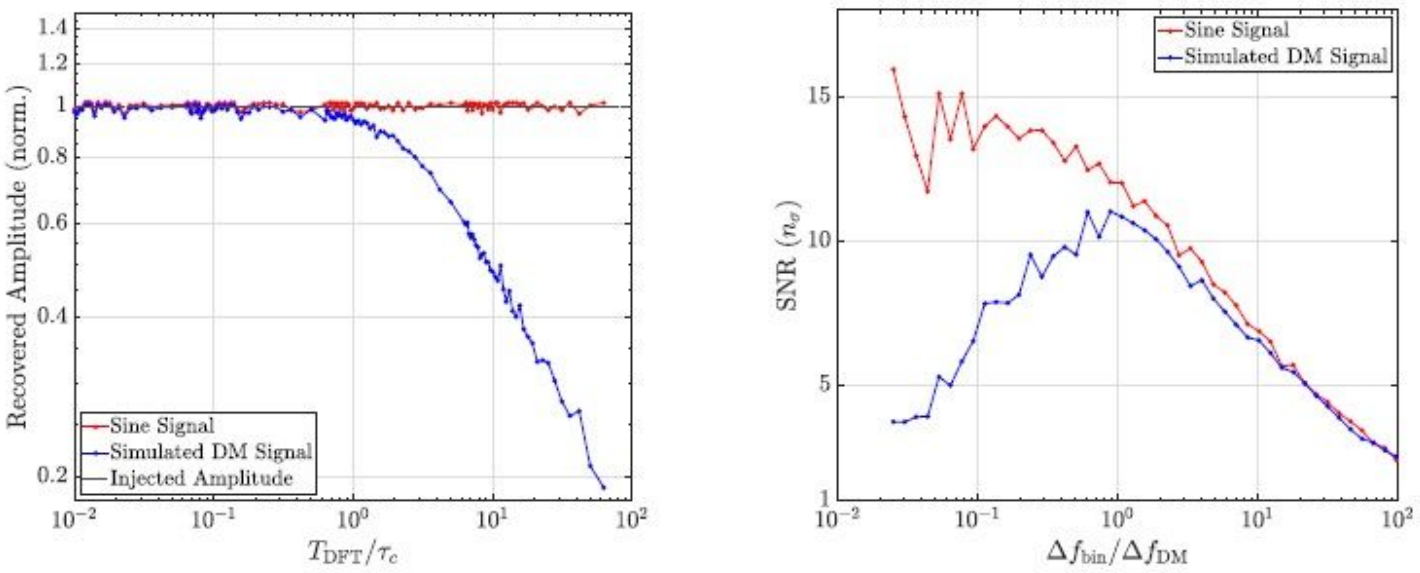

Figure 3

The spectral amplitude (left) and signal-to-noise ratio (SNR, right) of a simulated DM signal (blue) and monochromatic sine wave (red) as recovered from spectra created using different frequency bin widths (fbin = 1=TDFT). The plotted recovered amplitude is normalised by the injected amplitude. The SNR (n) is measured as the difference between the signal amplitude and the noise amplitude divided by the standard deviation of the noise. The appearance of a maximum for the SNR as shown on the right is a direct consequence of both the decrease of the recovered amplitude of signals with limited coherence (as shown on the left) and the scaling of white Gaussian noise with increasing integration time. The plot on the left was produced by injecting a simulated dark matter signal and a perfect sine into a segment of GEO600 data and creating spectra using the modified LPSD technique described above. The plot on the right was made by injecting the same signals into white Gaussian noise and creating spectra using Welch's method. Note that for any single bin and for equal TDFT the spectral estimate obtained with the LPSD method (Eq. 6) is mathematically equal to that obtained with Welch's method.